ADVANCED FUNCTIONAL MATERIALS
www.afm-journal.de

Structure-Performance Relationship of Aromatic Polymer Binder for Silicon Anode in Lithium-Ion Batteries

Junho Kim, Gyuri Kim, You Kyung Park, Gayoung Lim, Seung Tae Kim, In Hwan Jung, and Hansu Kim**

Polymer binders are essential for Silicon (Si) anode-based lithium-ion batteries (LIBs). However, the synthetic guidance for aromatic polymer binder is relatively less explored compared to aliphatic polymer binders. In this study, polyimide-based aromatic polymer binders are developed that have strong binding affinity with Si particles, a conductive agent and copper (Cu) current collector, and they show an improved initial discharge capacity of 2663 mAh g^{-1}, which is 29% higher than that of Kapton-based one (2071 mAh g^{-1}). The copolymerization between "hard" and "soft" segments is crucial to achieve reversible volume expansion/contraction during the repeated charging/discharging process, resulting in the best cycle performance. The new binder ensures both excellent volume retention after full-delithiation and allowed volume expansion at least to some extent upon full-lithiation. This Study finds a power-law relationship between the capacity of Si anode and the mechanical properties of the binder, i.e., the tensile stress (σ) and strain (ε). The initial discharge capacity is proportional to $\sigma^n \cdot \varepsilon$ (n = 2.3–2.7). Such an understanding of the relationships between polymer structure, mechanical properties of the polymer and binder performance clearly revealed the importance of the soft-hard polymer structure for aromatic binders used in Si-based high-capacity lithium storage materials.

1. Introduction

Lithium-ion batteries (LIBs) are fast-growing electrical energy storage systems widely utilized in wireless electronic devices and vehicles due to their high energy density and excellent charge/discharge efficiency. As the use of LIBs has become more popular, the demand for longer-lasting batteries has grown rapidly.[1–3] Currently, the specific capacity of the anode used in commercialized LIBs almost reached the theoretical maximum limit of graphite (372 mAh g^{-1} for LiC_6.).[4–7] It is necessary to explore alternative anode materials to further improve the energy density of LIBs, and Si-based anode materials are regarded as some of the best solutions because of the high theoretical capacity of Si (3579 mAh g^{-1} for $Li_{3.75}Si$).[8–11] However, Si has critical problems due to repeated volume expansion and contraction during the charging and discharging processes, respectively, which deteriorates the mechanical and electrical properties of Si anode, eventually resulting in poor capacity retention.[12–14] The development of polymer binders that can effectively suppress volume expansion of Si particles as well as allow reversible volume recovery during cycling is the key for the success of LIBs adopting Si-based anode materials.[15–18]

Various types of polymeric binders based-on biomass, polyols, polyacrylic acids, polyamide imides and polyimides have been developed, and crucial synthetic strategies have been discovered.[19–27] First, polymer binders should possess functional groups capable of strongly bonding with Si particles. For this reason, hydroxy, amino and carboxylic groups are commonly observed in the polymer binders.[28–30] Second, there should be strong intermolecular interactions between polymer chains that resist the volume expansion of Si particles.[31,32] In the case of aliphatic polymer binders, crosslinking or supramolecular structures are introduced to suppress the volume expansion of the Si particles because the polymer backbone is soft.[33–36] Liu et al. reported an in situ covalently bonded cross-linking network polymer binder consisting of PAA with carbonyl groups and isocyanate-terminated polyurethane oligomers (PUOs), and 2-ureido-4-pyrimidinone (UPy) as reversible quadruple hydrogen bonding cross-linkers for Si anodes in LIBs.[37] Choi et al. reported polyrotaxanes as sliding motion crosslinking network polymer binders with integrated PAA as a linear polymer and β-cyclodextrin (CD) as a ring-shaped supramolecular structure.[38] Conversely, crosslinking is rarely observed in the case of aromatic polymers, probably because the polymer backbone is rigid and there are strong π–π stacking interactions between polymer chains. However, we do not yet understand how soft or how hard the aromatic polymers must be to realize reversible volume

J. Kim, Y. K. Park, G. Lim, S. T. Kim, H. Kim
Department of Energy Engineering
Hanyang University
222 Wangsimni-ro, Seongdong-gu, Seoul 04763, Republic of Korea
E-mail: khansu@hanyang.ac.kr
G. Kim, I. H. Jung
Department of Organic and Nano Engineering
and Human-Tech Convergence Program
Hanyang University
222 Wangsimni-ro, Seongdong-gu, Seoul 04763, Republic of Korea
E-mail: inhjung@hanyang.ac.kr
The ORCID identification number(s) for the author(s) of this article can be found under https://doi.org/10.1002/adfm.202303810

DOI: 10.1002/adfm.202303810

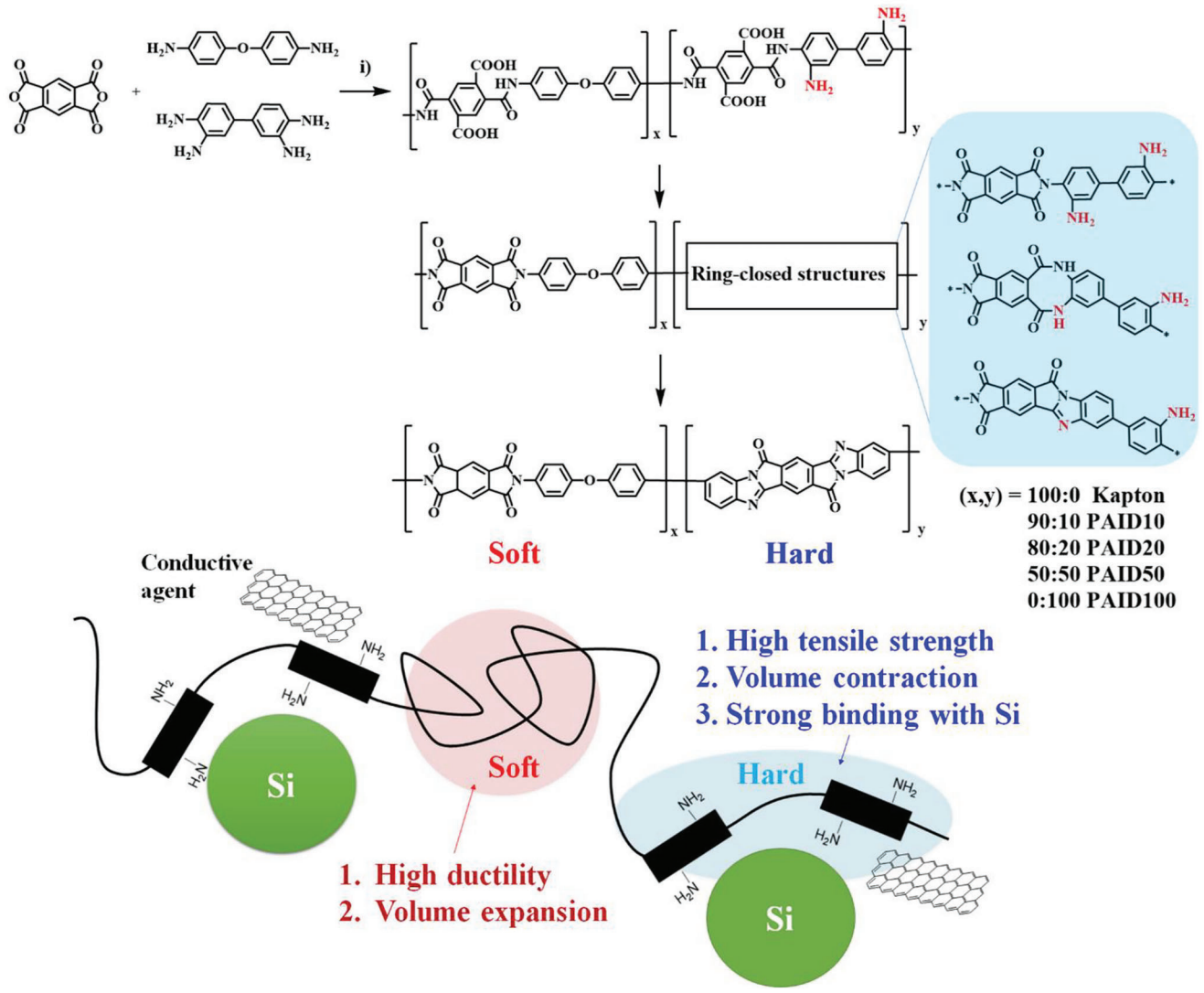

Scheme 1. Synthesis of PAID binders. Reaction conditions: i) DMF, rt, 12 h.

recovery during the repeated volume expansion and contraction of Si anodes.

In this study, we suggest a new synthetic strategy for the aromatic polymer binder that can efficiently respond to repeated volume expansion and contraction of Si-anode for LIBs by understanding the relationships between polymer structure, mechanical properties of the polymer and binder performance. Aromatic polymers have a rigid and ordered backbone structure, which increases tensile strength of the polymers.[39–41] This high tensile strength is a crucial factor to reduce the volume expansion of Si particles, resulting in minimal volume change during the charging/discharging process.[22,42] However, if the tensile strength is too high, the polymer loses its elasticity, which means that it can no longer function as a binder. Thus, a new strategy is needed to 1) suppress severe volume expansion during the charging process but also 2) allow efficient volume expansion/contraction during charging/discharging over a full cycle at the same time.

Poly(4,4′-oxydiphenylene-pyromellitimide) (trade name: Kapton) polymerized from pyromellitic dianhydride and 4,4′-diaminodiphenyl ether monomers was selected as a control aromatic polymer binder due to its promising binder properties and versatility.[23,43,44] Molecular engineering of this representative aromatic polymer can be expanded to provide general synthesis guidance to develop high-performance aromatic polymer binders.[45] To improve binding properties of the Kapton structure, 3,3′-diaminobenzidine monomer was introduced in a Kapton polymer backbone as an third component. The 3,3′-diaminobenzidine moiety has four amine functional groups and can form heterocyclic aromatic backbone structure by imidazolation, which effectively increases the binding to both Si particles and the conductive agent (like carbon black particles) as well as hardness of the polymer backbone (**Scheme 1**). Thus, a 3,3′-diaminobenzidine moiety forms "hard" segments in a polymer backbone, whereas a relatively flexible 4,4′-diaminodiphenyl ether moiety serves as a "soft" segment in a polymer binder. The control of feed ratio among pyromellitic dianhydride, 4,4′-diaminodiphenyl ether (soft segment), and 3,3′-diaminobenzidine (hard segment) monomers could make the

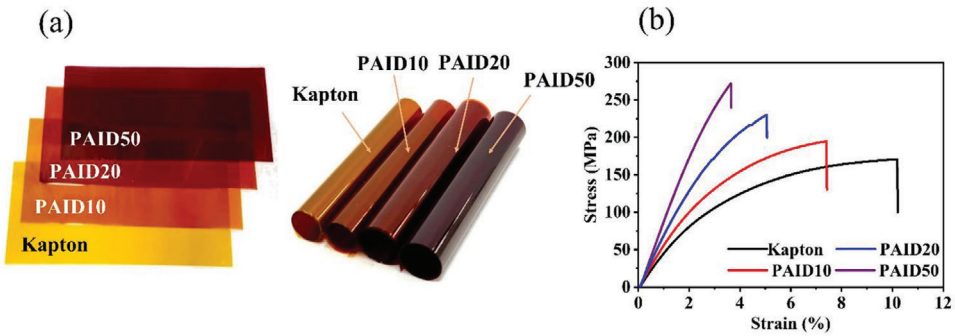

Figure 1. a) Free-standing films of Kapton, PAID10, PAID20, and PAID50. b) Stress-strain curves of corresponding free-standing films.

balance between hardness and softness of the polymer binder, thereby achieving effective suppression of the volume expansion of Si particles as well as enabling reversible volume recovery during cycling at the same time. Five copolymers composed of pyromellitic dianhydride, 4,4′-diaminodiphenyl ether, and 3,3′-diaminobenzidine monomers were synthesized by adjusting ratio of soft-hard segments. Their feed ratios were controlled as 100:100:0, 100:90:10, 100:80:20, 100:50:50, and 100:0:100, and the resulting polymers were referred to as Kapton, PAID10, PAID20, PAID50, and PAID100, respectively. As the amount of 3,3′-diaminobenzidine increased in a polymer, the tensile strength of the polymer rapidly increased, which effectively suppressed the volume expansion of the Si anodes. Interestingly, PAID20 binder containing only 20% 3,3′-diaminobenzidine exhibited the highest initial discharge capacity of 2663 mAh g^{-1}, which was 29% higher than that of the Kapton-based Si anode (2071 mAh g^{-1}). PAID20-based Si anode also showed the best cycle performance among the synthesized polymer binders. We found that both the tensile stress (σ) and strain (ε) of the polymers were closely related to binder performance, and the initial discharge capacity c) was proportional to $\sigma^n \cdot \varepsilon$ (n = 2.3–2.7). This indicates that the balance between tensile strength and ductility is highly important in aromatic polymer binders and that tensile strength is a more dominant parameter than ductility. Imparting both hardness and softness in a polymer binder is crucial to improve the LIB performance.

2. Results and Discussion

2.1. Synthesis and Characterization of Materials

The polymer binders were synthesized via terpolymerization of three monomers, pyromellitic dianhydride, 4-aminophenyl ether and 3,3′-diaminobenzidine (Scheme 1). The ratio of pyromellitic dianhydride was fixed at 1.0, and the ratio of 4-aminophenyl ether and 3,3′-diaminobenzidine was controlled to be 1.0:0, 0.9:0.1, 0.8:0.2, 0.5:0.5, and 0:1.0, and the corresponding polymers were named Kapton, PAID10, PAID20, PAID50, and PAID100, respectively. We anticipated that introducing 3,3′-diaminobenzidine into the aromatic polyimides would serve dual functions.[46] First, the extra amines can provide strong binding with Si particles after imidization. Second, the remaining amines that do not bind with Si make fused aromatic rings after thermal imidazolation, which enhances the interactions with the conductive agent. Thus, increasing 3,3′-diaminobenzidine in a Kapton structure can improve binding properties with both Si particles and the conductive agent. To understand the effect of 3,3′-diaminobenzidine on the mechanical property of the polymers, their tensile strengths were measured using free-standing polymer films (**Figure 1**a). Figure 1b shows the stress–strain curves of Kapton, PAID10, PAID20, and PAID50 free-standing films. Note that PAID100 film was not possible due to its brittleness. The tensile stresses of Kapton, PAID10, PAID20, and PAID50 were 170, 194, 230, and 272 MPa, respectively, and the corresponding tensile strains were 10.2, 7.4, 5.0, and 3.6%, respectively. As the amount of 3,3′-diaminobenzidine increased, the tensile strength showed a gradual increase, while the ductility decreased. These results revealed that the 3,3′-diaminobenzidine segment is a hard segment, whereas 4-aminophenyl ether segment is a soft segment in the polymer. As we anticipated, this terpolymerization employing the soft and hard segments helped control the mechanical properties of the polymers. The schematic description of the "soft/hard" concept of the polymer binders were shown in Scheme S1 (Supporting Information).

The molecular weights of all the synthesized polymers were estimated by gel-permeation chromatography (GPC) using Dimethylformamide (DMF) eluent at room temperature. The number-average molecular weight ($\overline{M_n}$) of Kapton, PAID10, PAID20, PAID50, and PAID100 were 1657, 307, 209, 218, and 213 kDa, respectively, and the corresponding weight-average molecular weight ($\overline{M_w}$) were 2960, 567, 382, 882, and 4220 kDa, respectively (Figures S1–S5, Supporting Information). All the polymers showed significant molecular weights. Fourier transform infrared spectroscopy (FT-IR) of the polymers showed characteristic peaks for C–N–C symmetric, C=O symmetric, and asymmetric stretching at 1356–1374, 1710–1729 cm^{-1}, and 1751–1776 cm^{-1}, respectively, which indicated successful synthesis of polyimides (Figures S7–S11, Supporting Information).

Peel tests of the Si anodes were conducted to compare the adhesion forces of the synthesized polymer binders based on the ratio of 3,3′-diaminobenzidine. **Figure 2**a shows that the average adhesion force gradually increased in order of Kapton (4.21 N) < PAID10 (7.81 N) < PAID20 (9.08 N) < PAID50 (9.58 N) < PAID100 (10.43 N), and these results are compared to the peel test results of the pristine polymer binder film coated on the Cu current collector (Figure 2b). The average adhesion force between the Cu current collector and the binder similarly increased in the order of Kapton (0.86 N) < PAID10

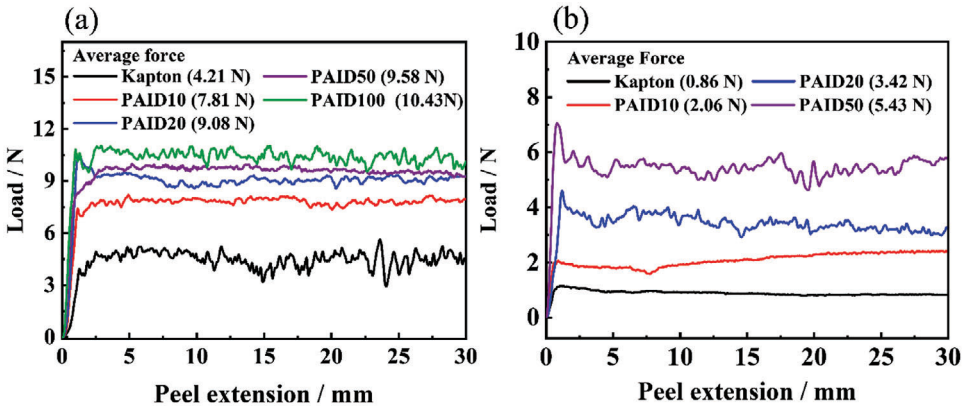

Figure 2. The peel test of a) electrode composed of Si anode materials, conductive additive, and binder and b) pristine binder on Cu current collector.

(2.06 N) < PAID20 (3.42 N) < PAID50 (5.43 N). These results indicate that the incorporation of 3,3′-diaminobenzidine in a polymer backbone both improved the interaction with Si particles and conductive agents and effectively suppressed the delamination from the Cu current collector. Overall, we concluded that the increase of 3,3′-diaminobenzidine in a polymer backbone improved the binding properties with both Si particles and conductive agent as well as enhanced the tensile strength of the polymer.

2.2. Binder Properties in Li-Ion Batteries

The electrochemical performance of Si anode was investigated for polymer binders with different ratios of hard-soft segments. **Figure 3**a shows the first charge–discharge potential profile of the Si anodes with different polymer binders. Kapton, PAID10, PAID20, PAID50 and PAID100-based Si anodes showed initial charge (lithiation) capacities of 3274, 3190, 3526, 3221, and 3233 mAh g^{-1}, respectively, at a rate of 0.2 C, and the corresponding initial discharge (delithiation) capacities of 2071, 2373, 2663, 2351, and 2459 mAh g^{-1}, respectively. The initial Columbic efficiency (ICE) of Si anodes with polymers binders containing 3,3′-diaminobenzidine was 73–76%, which was much higher than that of Si anode with a Kapton binder (63%). Such an improvement in the reversible capacity and ICE of the Si anode was mainly due to the improved the binding properties with both Si particles and conductive agents by introducing 3,3′-diaminobenzidine moieties in a polymer backbone. Notably, the PAID20-based Si anode exhibited the best charge and discharge capacity among the Si anodes with polymer binders. These results suggest that the optimal amount of hard segments in a polymer backbone is near 20%, suggesting that the balance between soft and hard segments in a polymer chain is one of the most important factors for aromatic polymer binders. We tried to find a relationship between the mechanical properties of the polymers (tensile strength and ductility) and the reversible capacity of the Si anode. As shown in **Figure 4**, we found that there was a power-law relationship between the capacity of Si anode and the mechanical properties of the binder, i.e., the tensile stress (σ) and strain (ε). As shown in Figure 4 and Equation (1), the initial discharge capacity (C) was proportional to $\sigma^n \cdot \varepsilon$ (n = 2.3–2.7).

$$C \propto \sigma^n \cdot \varepsilon \quad (n = 2.3 - 2.7) \tag{1}$$

Since the discharge capacity is expressed by the product of tensile stress and strain, increasing both tensile strength and ductility is the key to maximizing the binder performance. In addition, tensile strength was the dominant parameter for increasing the reversible capacity of Si anode because n is >1. As discussed before, the hardness and softness of the polymer chains are closely related to tensile strength and ductility, respectively. Thus, incorporation of both hard and soft segment in a polymer backbone is a highly effective way to maximize the capacity of the Si anode.

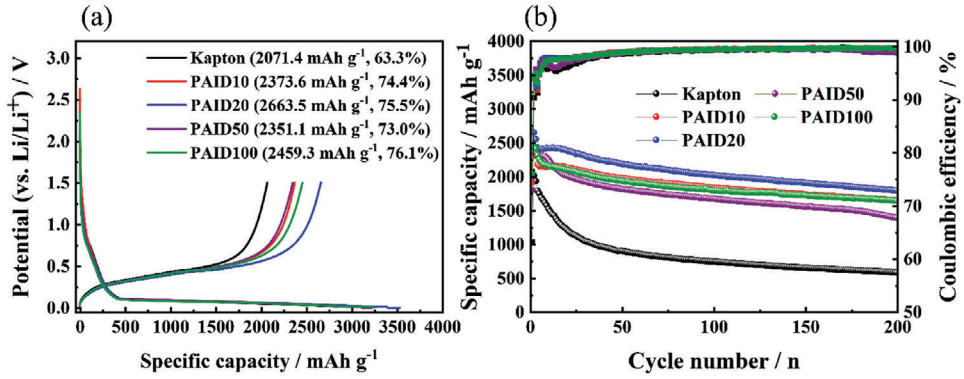

Figure 3. a) The charge–discharge voltage profile and b) electrochemical cycle performance of a Si anode with different binders.

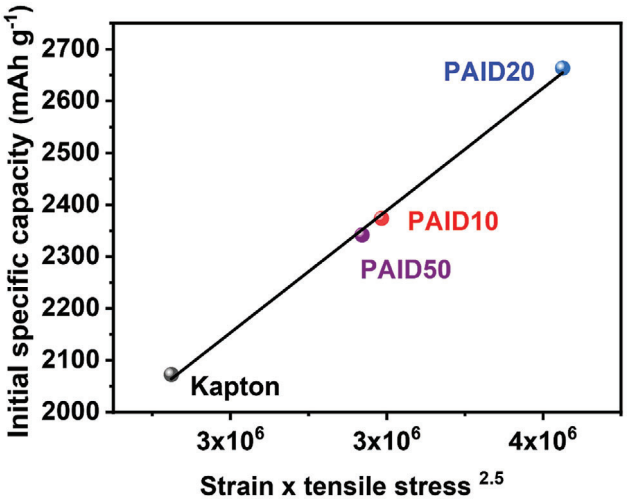

Figure 4. The power-law relationship between the capacity of Si anode and the mechanical properties of the binder, i.e., the tensile stress (σ) and strain (ε).

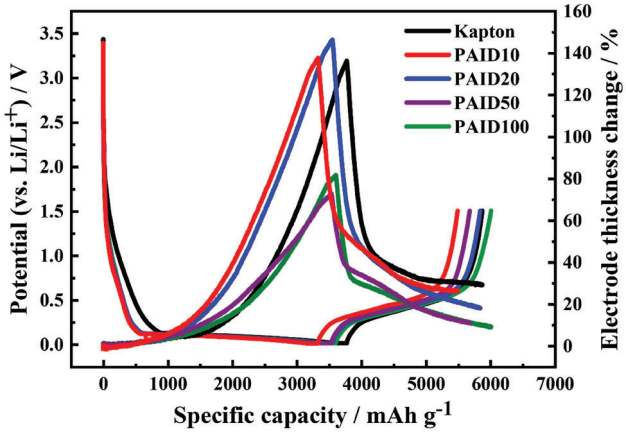

Figure 5. In situ electrochemical dilatometric analysis of Si anode for various binders during the 1st cycle.

Figure 3b shows the cycle performance of the Si anodes with the polymer binders during 200 cycles at a rate of 0.2 C. The discharge capacity of Si anode with Kapton rapidly decreased within 50 cycles, while the Si anodes with PAID binders exhibited much improved capacity retention over 200 cycles. This implies that the polymer binders containing 3,3′-diaminobenzidine are highly effective in reducing the structural deformation of the Si anode by suppressing volume expansion and reversible volume recovery against the repeated volume expansion and contraction of Si during cycling. Like the capacity and ICE, the PAID20-based Si anode showed the best cycle performance, also revealing the importance of soft-hard balance in a polymer binder.

In situ electrochemical dilatometer measurements were made to validate the effect of volume suppression of the Si anode with 3,3′-diaminobenzidine. **Figure 5** shows a real time dilatometric profile of the Si anodes in the first cycle. The height expansion rates of the Si anode with Kapton, PAID10, PAID20, PAID50, and PAID100 were 136, 137, 146, 72, and 81%, respectively, after the full lithiation process, and the corresponding volume contraction percentages were 108, 112, 129, 62, and 73%, respectively, after the full delithiation process. Upon lithiation, the Si anode with the binders having a lower relative amount of 3,3′-diaminobenzidine moieties (10–20%) showed greater expansion even than the Si anode with Kapton binder, while the volume expansion rates were dramatically suppressed for the Si anodes with a higher relative amount of 3,3′-diaminobenzidine moieties (>50%). Similarly, the Si anode with the lower relative amount of 3,3′-diaminobenzidine moieties (10–20%) showed greater contraction than other Si anodes. These results can be explained by the differences between the mechanical properties of the polymer binders with 3,3′-diaminobenzidine moieties. Soft and elastic binders with lower relative amounts of 3,3′-diaminobenzidine moieties (10–20%) showed large volume expansion and contraction, while more rigid and less elastic binders with a relatively higher amount of 3,3′-diaminobenzidine moieties (50–100%) suppressed the volume expansion and contraction of the Si anode. Volume retention percentage was estimated by comparing the volume differences before and after full charge/discharge. The volume retention percentages of Si anode with Kapton, PAID10, PAID20, PAID50, and PAID100 were 80%, 82%, 89%, 86%, and 90%. PAID50 and PAID100 anodes showed excellent volume retention percentages higher than 86%, mainly due to their smaller volume expansion upon the lithiation process, while Kapton and PAID10 anode showed relatively poor volume retention of ≈80%. These results suggest that the small amount of 3,3′-diaminobenzidine moieties (0–10%) in a polymer backbone is not enough to promote volume retention during cycling. The PAID20 anode showed a volume retention of 89%, which is almost the same value as those of PAID50 and PAID100. Interestingly, PAID20 binder showed two sharply contrasting aspects of behavior upon lithiation and delithiation. The volume expansion behavior of PAID20 resembled Kapton and PAID10, but the volume retention behavior of PAID20 was similar to PAID50 and PAID100. This indicates that PAID20 possessed the best mechanical properties as a binder for Si anode among the synthesized binders due to the well-balanced soft and hard segment in the polymer backbone. The soft segments allow volume expansion during the lithiation, and the hard segments provide excellent volume recovery via the strong intermolecular interactions with both Si particles and conductive agents. Increasing the relative amount of hard segments in a polymer backbone might be an effective way to improve the volume retention property of Si anodes. However, one cannot rule out the possibility that the mechanical stress exerted on the Si anode upon lithiation can increase due to small strain of the polymer binders with an increase in hard segments in a polymer backbone. Both the volume retention rate of Si anode after delithiation and its volume expansion upon full lithiation should be considered at the same time for a more ideal design of polymer binders for Si anodes. This means that better binders could both enable the excellent volume retention after full delithiation and allow the volume expansion (at least to some extent) upon full lithiation, thereby relieving the mechanical stress exerted on the polymer binder. In this regard, PAID20 showed well-balanced binder performance for a Si anode that undergoes repeated volume expansion and contraction.

Figure 6a shows the electrical resistance for composite layer in the Si anode composed of Si nanoparticles, conductive agent, and polymer binder. The average composite layer resistances of

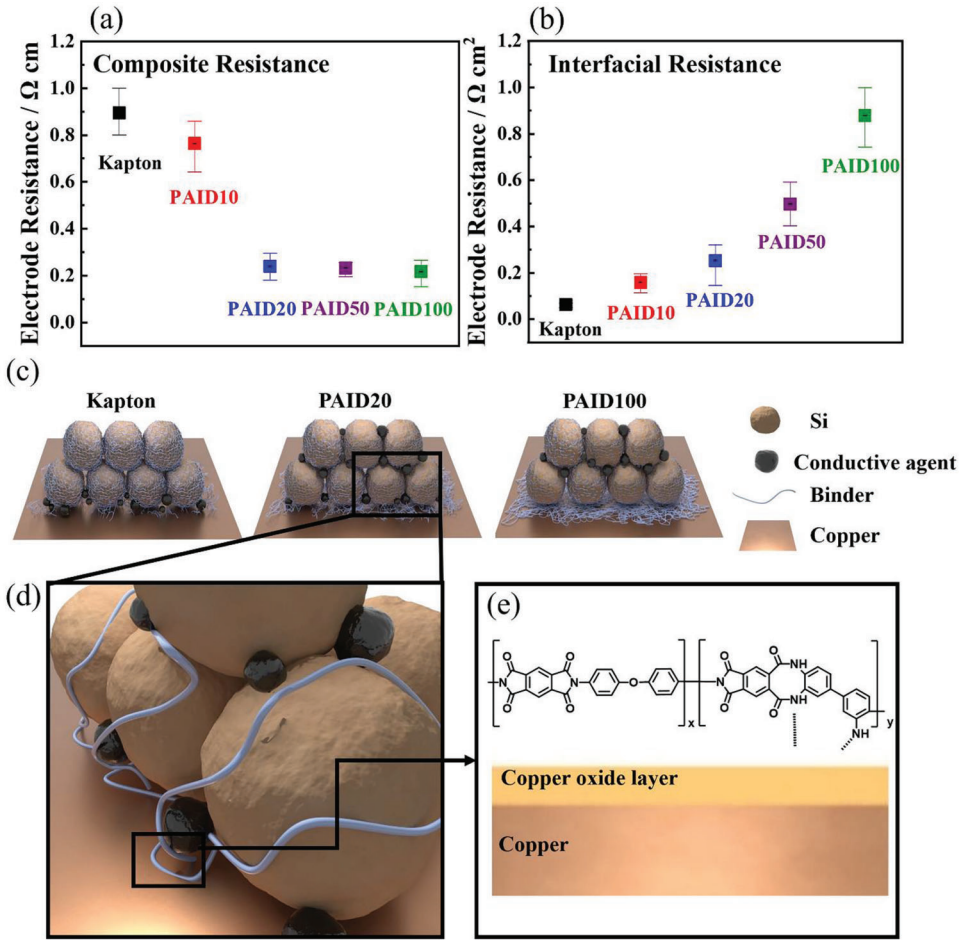

Figure 6. a) Composite resistance of Si anode materials, conductive additive, and binder composite electrode, and b) interfacial resistance between the composite layer and Cu current collector. c) Schematic illustration of Si anode with different binders, d) schematic illustration of Si anode at different magnifications, and e) binding interactions between binder and Cu current collector.

Kapton, PAID10, PAID20, PAID50, and PAID100-based Si anode were 0.895, 0.764, 0.239, 0.232, and 0.216, respectively, which showed an inverse relationship with the relative amount of 3,3′-diaminobenzidine in the polymer. Interestingly, the composite layer resistance of Si anode dramatically decreased at the PAID20 anode and retained similar values to PAID50 and PAID100 containing the higher ratio of 3,3′-diaminobenzidine. This implies that the critical amount of 3,3′-diaminobenzidine in a polymer backbone would be near 20% for well-balanced tensile strength and ductility while maintaining efficient intermolecular interactions with Si particles and a conductive agent.

The average interfacial resistances between the composite layer and Cu current collector of Kapton, PAID10, PAID20, PAID50, and PAID100-based Si anodes were 0.063, 0.159, 0.253, 0.497, and 0.878, respectively (Figure 6b). Interfacial resistance gradually increased as the relative amount of 3,3′-diaminobenzidine in a polymer binder increased. The increase in 3,3′-diaminobenzidine in a polymer binder improved the binding affinity of the composite layer with the Cu current collector, thereby leading to the increase in the interfacial resistance of Si anode (Figure 6c–e). One can reasonably expect that such an enhancement in the binding affinity of PAID binders by the increase of 3,3′-diaminobenzidine moiety can boost the average adhesion force between the Cu current collector and Si anode, which was confirmed by the peel test of Si anodes as shown in Figure 2a.

The rate capability of Si electrode was measured as shown in Figure S14 (Supporting Information). The rate capability is increasing as the amount of "hard" segment is increasing in a polymer chain. This indicates that there was close relationship between binding forces and rate capability, and the higher adhesion forces of polymer binder can enhance the rate capability of the Si electrode. However, PAID20 having moderate binding forces between Cu current collector and Si anode showed the comparable rate capability with PAID100 having the highest adhesion forces and interfacial resistances. This means that PAID20, which balances tensile strength and ductility, has the advantage of improving both specific capacity and cycle stability.

3. Conclusion

We proposed polyimide-based aromatic polymers composed of pyromellitic dianhydride, 4-aminophenyl ether (soft segment), and 3,3′-diaminobenzidine (hard segment) as a binder material

for Si-based high-capacity anode in LIBs. The introduction of a hard segment (3,3′-diaminobenzidine) in a polymer backbone significantly enhanced the binding affinity of the binders with Si particles, conductive agent and Cu current collector at once. This resulted in significant improvement in the initial discharge capacity of Si anode from 2071 mAh g^{-1} to 2663 mAh g^{-1} with an enhanced initial columbic efficiency from 63% to 76%. We found that there is an optimal hard-soft segment ratio for both discharge capacity and cycle performance at 20% of hard segments (PAID20 anode). The real-time dilatometric profile of the Si anodes revealed that that PAID20 showed excellent volume retention after full delithiation and allowed the volume expansion (at least to some extent) upon full lithiation, thereby relieving the mechanical stress exerted on the polymer binder. These results suggested that the rational design in the soft and hard segments ratio was crucial to achieve this ideal binder behavior. Specifically, the soft segments allow volume expansion upon lithiation, while the hard segments facilitate volume recovery via strong intermolecular interaction with both Si particles and conductive agents. We discovered that there is a power-law relationship between the capacity of the Si anode and the mechanical properties of the binder, i.e., the tensile stress (σ) and strain (ε). The initial discharge capacity was proportional to $\sigma^n \cdot \varepsilon$ (n = 2.3–2.7). This finding suggests that imparting both hardness and softness to a polymer binder is necessary to improve the electrochemical performance of the Si anode. In addition, the balance between tensile strength and ductility is highly important in aromatic polymer binders and tensile strength is a more dominant parameter than ductility. Understanding the relationships between polymer structure, mechanical properties of the polymer and binder performance will help in the development of high-performance aromatic polymer binders for Si-based high-capacity anode materials.

4. Experimental Section

General Polymerization: The polymer binders were synthesized by the copolymerization of pyromellitic dianhydride, 4,4′-diaminodiphenyl ether, and 3,3′-diaminobenzidine monomers. Their feed ratios were 100:100:0, 100:90:10, 100:80:20, 100:50:50 and 100:0:100, and the resulting polymers were referred to as Kapton, PAID10, PAID20, PAID50 and PAID100, respectively. 3,3′-Diaminobenzidine and 4,4′-diaminodiphenyl ether were added into a 100 ml two-necked round-bottom flask in a nitrogen atmosphere and were dissolved in DMF (20 ml). Pyromellitic dianhydride (5.78 mmol, 1.55 g) in DMF (15 ml) was added dropwise into the solution at 0 °C, and the mixture was stirred at room temperature for 12 h. The crude polymer was precipitated out from the reaction mixture by the treatment of diethyl ether and water, and then solid residue was dried under vacuum at room temperature. The polymer obtained was a brown solid and was used directly without further purification.

Characterization of the Binder and Electrode Materials: Fourier transform infrared (FT-IR) spectra were recorded on a Nicolet 6700 FT-IR Spectrometer (Thermo Scientific). Thermogravimetric analysis (TGA) was observed with a SDT Q600 (TA Instruments) at a scanning rate of 10 °C/min in an air atmosphere. Gel permeation chromatography (GPC) was conducted at room temperature using dimethylformamide as the eluent. The peel-off test was measured using a 3 kgf load-cell with a TXA Multi-axis Micro-Texture Analyzer (YEONJIN S-Tech). Electrode resistance was conducted with an Electrode Resistance Measurement System RM2610 (Hioki). The morphology and microstructure of the active materials were examined using a field-emission scanning electron microscope (FESEM, JEOLJSM-7000F, Akishima, Japan).

Electrochemical Measurements: The synthesized polyamic acid powders were dissolved in NMP 15,16 wt.% for preparation of the electrodes. The silicon anodes were prepared using a slurry composed of 60% nano silicon, 20% Super P, and 20% binder dissolved in NMP, which was coated onto Cu foil using a doctor blade. The cast slurries were heated to 80 °C for 1 h and then dried at 200 °C under vacuum for 2 h. The active mass loading of all electrodes was ≈0.42 ± 0.05 mg cm^{-2} based on the Si content in the electrode. The Si anode was cut into 1.1 cm^2 pieces as working electrodes, and the coin cells were assembled as CR2032 types with polypropylene as the separator and Li metal as the counter electrode. The electrolyte consisted of 1 M $LiPF_6$ in EC/EMC = 3/7 (v/v), and 5.0 wt.% of fluoroethylene carbonate (FEC) (Panax EtecCo. Ltd. South Korea) was added into the coin cell. All coin cells were fabricated in an Ar-purging glove box. The coin cells were tested in constant current-constant voltage (CC-CV) mode in a voltage range of 0.005–1.5 V (vs Li/Li^+) at room temperature with a current density of 0.2C (1C = 3,579 mA g^{-1}).

In situ Dilation Change Analysis: An in situ electrochemical dilatometer (ECD-3, EL-Cell) was employed to measure the dilation change of the silicon anode with a Kapton or PAID binders. The working electrode was separated from the counter electrode by a rigid glass frit, which was fixed in position. The working electrode was sealed by means of a thin metal foil, which transmits electrochemical reaction-induced thickness changes toward the sensor unit above. Dimensional changes in the ≈100 nm–500 µm range were detected by a high-resolution sensor (LVDT sensor with < 50 nm resolution). The load on the sensor was fixed at 1.0 N. In this study, Si anodes were used as the working electrode with a diameter of 9 mm, and Li metal was used as a counter electrode (diameter: 11 mm). The hole of the reference pin was filled with lithium metal to construct the reference electrode. Thickness variation of the working electrode was expressed in percent change of the thickness of the pristine electrode excluding the thickness of the current collector. Thickness of pristine electrode was measured using a micrometer (MDH-25 MB, Mitutoyo). The assembled in situ electrochemical dilatometer cells were tested in a constant current-constant voltage (CC-CV) mode in a voltage range of 0.005–1.5 V (vs Li/Li^+) at room temperature at a rate of 0.05 C (1 C = 3579 mA g^{-1}) with an electrolyte of 1.5 M $LiPF_6$ dissolved in a mixture of ethylene carbonate (EC) and dimethyl carbonate (DMC) (3:7, v/v) with 5.0 wt.% fluoroethylene carbonate (FEC) (Panax Etec. Co. Ltd.).

Fabrication of Free-Standing Polyimide Film: The synthesized polyamic acid powders dissolved in NMP 15,16 wt.% for fabrication of free-standing polyimide film. The polyamic acid solution was cast onto a clean glass plate using a doctor blade, and the resulting film was dried inside a vacuum oven at 50 °C/ 760 Torr/ 2 h, 80 °C/ 1 Torr/ 1 h, 120 °C/ 0.5 Torr/ 1 h, and 200 °C/ 0.5 Torr/ 2 h. The resulting polyimide film typically showed a thickness of 25 ± 5 µm.

Supporting Information

Supporting Information is available from the Wiley Online Library or from the author.

Acknowledgements

This research was supported by Basic Research Program through the National Research Foundation of Korea (NRF) grant funded by the Korean government (MSIT) (NRF-2021R1A2C2013135), and also supported by the research fund of Hanyang University (HY- 202200000003364).

Conflict of Interest

The authors declare no conflict of interest.

Data Availability Statement

The data that support the findings of this study are available from the corresponding author upon reasonable request.

Keywords

Li-ion batteries, polymer binders, silicon anodes, soft-hard copolymers, tensile stress-strain relationship

Received: April 6, 2023
Revised: June 9, 2023
Published online: July 4, 2023

[1] M. Armand, J.-M. Tarascon, *Nature* **2008**, *451*, 652.
[2] Y. Sun, Z. Yang, L. Gu, Y. Chen, H. Zhou, *Joule* **2018**, *2*, 1265.
[3] X. Jiao, J. Yin, X. Xu, J. Wang, Y. Liu, S. Xiong, Q. Zhang, J. Song, *Adv. Funct. Mater.* **2021**, *31*, 2005699.
[4] X. Zeng, M. Li, D. Abd El-Hady, W. Alshitari, A. S. Al-Bogami, J. Lu, K. Amine, *Adv. Energy Mater.* **2019**, *9*, 1900161.
[5] B. L.-H. Hu, F.-Y. Wu, C.-T. Lin, A. N. Khlobystov, L.-J. Li, *Nat. Commun.* **2013**, *4*, 1687.
[6] L. Zhao, B. Ding, X. Y. Qin, Z. Wang, W. Lv, Y. B. He, Q. H. Yang, F. Kang, *Adv. Mater.* **2022**, *34*, 2106704.
[7] S. Xu, J. Zhou, J. Wang, S. Pathiranage, N. Oncel, P. R. Ilango, X. Zhang, M. Mann, X. Hou, *Adv. Funct. Mater.* **2021**, *31*, 2101645.
[8] K. Ogata, S. Jeon, D.-S. Ko, I. Jung, J. Kim, K. Ito, Y. Kubo, K. Takei, S. Saito, Y.-H. Cho, *Nat. Commun.* **2018**, *9*, 479.
[9] K. Ogata, D.-S. Ko, C. Jung, J.-H. Lee, S. Sul, H.-G. Kim, J. Seo, J. Jang, M. Koh, K. Kim, *Nano Energy* **2019**, *56*, 875.
[10] K. Ogata, E. Salager, C. Kerr, A. Fraser, C. Ducati, A. J. Morris, S. Hofmann, C. P. Grey, *Nat. Commun.* **2014**, *5*, 3217.
[11] E. Adhitama, F. Dias Brandao, I. Dienwiebel, M. M. Bela, A. Javed, L. Haneke, M. C. Stan, M. Winter, A. Gomez-Martin, T. Placke, *Adv. Funct. Mater.* **2022**, *32*, 2201455.
[12] A. Casimir, H. Zhang, O. Ogoke, J. C. Amine, J. Lu, G. Wu, *Nano Energy* **2016**, *27*, 359.
[13] X. Zuo, J. Zhu, P. Müller-Buschbaum, Y.-J. Cheng, *Nano Energy* **2017**, *31*, 113.
[14] H. Tian, H. Tian, W. Yang, F. Zhang, W. Yang, Q. Zhang, Y. Wang, J. Liu, S. R. P. Silva, H. Liu, *Adv. Funct. Mater.* **2021**, *31*, 2101796.
[15] H. Chen, M. Ling, L. Hencz, H. Y. Ling, G. Li, Z. Lin, G. Liu, S. Zhang, *Chem. Rev.* **2018**, *118*, 8936.
[16] T. Liu, Q. Chu, C. Yan, S. Zhang, Z. Lin, J. Lu, *Adv. Energy Mater.* **2019**, *9*, 1802645.
[17] Z. Li, Y. Zhang, T. Liu, X. Gao, S. Li, M. Ling, C. Liang, J. Zheng, Z. Lin, *Adv. Energy Mater.* **2020**, *10*, 1903110.
[18] H. Chen, Z. Wu, Z. Su, S. Chen, C. Yan, M. Al-Mamun, Y. Tang, S. Zhang, *Nano Energy* **2021**, *81*, 105654.
[19] H. Zhong, J. He, L. Zhang, *Polymer* **2021**, *215*, 123377.
[20] P. Parikh, M. Sina, A. Banerjee, X. Wang, M. S. D'Souza, J.-M. Doux, E. A. Wu, O. Y. Trieu, Y. Gong, Q. Zhou, *Chem. Mater.* **2019**, *31*, 2535.
[21] A. Magasinski, B. Zdyrko, I. Kovalenko, B. Hertzberg, R. Burtovyy, C. F. Huebner, T. F. Fuller, I. Luzinov, G. Yushin, *ACS Appl. Mater. Interfaces.* **2010**, *2*, 3004.
[22] N.-S. Choi, K. H. Yew, W.-U. Choi, S.-S. Kim, *J. Power Sources.* **2008**, *177*, 590.
[23] J. S. Kim, W. Choi, K. Y. Cho, D. Byun, J. Lim, J. K. Lee, *J. Power Sources.* **2013**, *244*, 521.
[24] Q. Zhang, F. Zhang, M. Zhang, Y. Yu, S. Yuan, Y. Liu, *ACS Appl. Energy Mater.* **2021**, *4*, 7209.
[25] S. Jiang, B. Hu, Z. Shi, W. Chen, Z. Zhang, L. Zhang, *Adv. Funct. Mater.* **2020**, *30*, 1908558.
[26] H. Y. Ling, L. Hencz, H. Chen, Z. Wu, Z. Su, S. Chen, C. Yan, C. Lai, X. Liu, S. Zhang, *Sustain. Mater. Technol.* **2021**, *28*, e00283.
[27] H. Y. Ling, C. Wang, Z. Su, S. Chen, H. Chen, S. Qian, D.-S. Li, C. Yan, M. Kiefel, C. Lai, S. Zhang, *Energy Environ Mater.* **2021**, *4*, 263.
[28] M. Jeena, J.-I. Lee, S. H. Kim, C. Kim, J.-Y. Kim, S. Park, J.-H. Ryu, *ACS Appl. Mater. Interfaces.* **2014**, *6*, 18001.
[29] B. Koo, H. Kim, Y. Cho, K. T. Lee, N. S. Choi, J. Cho, *Angew. Chem.* **2012**, *124*, 8892.
[30] J. Song, M. Zhou, R. Yi, T. Xu, M. L. Gordin, D. Tang, Z. Yu, M. Regula, D. Wang, *Adv. Funct. Mater.* **2014**, *24*, 5904.
[31] J. Feng, D. Wang, Q. Zhang, J. Liu, Y. Wu, L. Wang, *ACS Appl. Mater. Interfaces.* **2021**, *13*, 44312.
[32] L. Deng, Y. Zheng, X. Zheng, T. Or, Q. Ma, L. Qian, Y. Deng, A. Yu, J. Li, Z. Chen, *Adv. Energy Mater.* **2022**, *12*, 2200850.
[33] S. Chen, Z. Song, L. Wang, H. Chen, S. Zhang, F. Pan, L. Yang, *Acc. Chem. Res.* **2022**, *55*, 2088.
[34] T.-w. Kwon, Y. K. Jeong, E. Deniz, S. Y. AlQaradawi, J. W. Choi, A. Coskun, *ACS Nano* **2015**, *9*, 11317.
[35] J. Ryu, S. Kim, J. Kim, S. Park, S. Lee, S. Yoo, J. Kim, N. S. Choi, J. H. Ryu, S. Park, *Adv. Funct. Mater.* **2020**, *30*, 1908433.
[36] G. Zhang, Y. Yang, Y. Chen, J. Huang, T. Zhang, H. Zeng, C. Wang, G. Liu, Y. Deng, *Small* **2018**, *14*, 1801189.
[37] Z. Liu, C. Fang, X. He, Y. Zhao, H. Xu, J. Lei, G. Liu, *ACS Appl. Mater. Interfaces.* **2021**, *13*, 46518.
[38] S. Choi, T.-w. Kwon, A. Coskun, J. W. Choi, *Science* **2017**, *357*, 279.
[39] W. Jang, J. Seo, C. Lee, S. H. Paek, H. Han, *J. Appl. Polym.* **2009**, *113*, 976.
[40] X. Lei, M. Qiao, L. Tian, Y. Chen, Q. Zhang, *J. Phy. Chem. C.* **2016**, *120*, 2548.
[41] Q. Yang, X. L. Gao, H. Y. Wu, Y. Y. Cai, Q. G. Zhang, A. M. Zhu, Q. L. Liu, *J. Power Sources.* **2019**, *436*, 226856.
[42] S. Uchida, M. Mihashi, M. Yamagata, M. Ishikawa, *J. Power Sources.* **2015**, *273*, 118.
[43] Y. So, H.-S. Bae, Y. Y. Kang, J. Y. Chung, N. K. Park, J. Kim, H.-T. Jung, J. C. Won, M.-H. Ryou, Y. H. Kim, *Nanomaterials* **2021**, *11*, 3164.
[44] T. Zhu, T.-N. Tran, C. Fang, D. Liu, S. P. Herle, J. Guan, G. Gopal, A. Joshi, J. Cushing, A. M. Minor, *J. Power Sources.* **2022**, *521*, 230889.
[45] C.-T. Lin, T.-Y. Huang, J.-J. Huang, N.-L. Wu, M.-k. Leung, *J. Power Sources.* **2016**, *330*, 246.
[46] J. Kim, Y. K. Park, H. Kim, I. H. Jung, *Chem. Mater.* **2022**, *34*, 5791.